

Raman Spectroscopy of Graphene Nanoribbons: A Review

C. Casiraghi and D. Prezzi

Abstract In the last few years, several methods have been proposed for the production of ultra-narrow stripes of graphene, called graphene nanoribbons, which could find several applications in nano- and opto-electronics. However, every production method gives rise to different types of ribbons, in terms of structural quality, width, edge pattern, and type of functional groups. In this review, we compare the Raman spectrum of graphene nanoribbons produced by different techniques by focusing on the effect of different structural parameters, such as width and edge-patterns. Effects due to changes in the lateral dimension are also discussed by comparing the Raman spectrum of ultra-narrow graphene nanoribbons with the spectrum of polycyclic aromatic hydrocarbons and defective graphene.

1 Introduction

The outstanding properties of graphene make it a very attractive material for many applications, ranging from electronics to energy and health care [1]. In particular, graphene exhibits ambipolar field effect and has high-mobility charge carriers of unique relativistic nature [2]. However, the lack of a bandgap strongly restricts the use of graphene in field-effect transistors and opto-electronics. Graphene nanoribbons (GNRs), defined as nanometer-wide stripes of graphene, are expected to combine the unique properties of graphene with the presence of a finite bandgap, produced by quantum confinement [3]. Quantum mechanics predicts the gap of a material to inversely increase with its lateral dimension [3], which in the case of GNRs corresponds to their width (w). However, calculations have demonstrated that the GNRs' electronic properties strongly depend on both the width, sometimes

C. Casiraghi (✉)

School of Chemistry, University of Manchester, Manchester, UK
e-mail: cinzia.casiraghi@manchester.ac.uk

D. Prezzi (✉)

CNR-Nanoscience Institute, S3 Center, Modena, Italy
e-mail: deborah.prezzi@nano.cnr.it

defined as multiple of the N carbon dimer lines across the width-axis direction, and the specific atomic arrangement at the edges [4, 5]. The most studied edges are those obtained by following high-symmetry directions in the graphene lattice, i.e., zigzag (Z) and armchair (A) edges.

GNRs with well-defined physical properties, and therefore suitable for nano-electronics, are required to be very narrow ($w \ll 10$ nm) and atomically precise, in particular at the edges [4, 5]. However, the production of such GNRs is very challenging. Standard top-down approaches (e.g. lithography, etching, cutting of graphene) yield GNRs with moderate width (>10 nm) and provides only relatively poor control over the edges [6–11]. Since the atomic structure of GNR reproduces an unrolled single-walled carbon nanotube (CNT), chemical unzipping of CNTs has been widely used for GNR's production [12–22], but only very few works reported ribbons with width below 10 nm [12, 14]. Alternative methods rely on local probe lithography [23], and solution methods [24–26]. Epitaxial-based methods have been also reported [27–33], such as plasma and chemical vapor deposition (PCVD and CDV, respectively). Recently bottom-up techniques based on surface-assisted [34–36] or on solution-mediated [37–43] cyclo-dehydrogenation have enabled the production of ultra-narrow ($w \ll 10$ nm) and atomically precise GNRs. The main advantage of the bottom-up methods compared to other techniques relies on the ability to determine the precise ribbons geometry by designing the structure of the molecular precursors on purpose. Note that in the case of solution-mediated GNRs the edges are typically functionalized by alkyl chains to provide a better solubility and to keep the ribbons planar [40].

Every production method gives rise to ribbons with very different structures, in term of width, length, edge morphology, position, and type of functional groups. Therefore, characterization is crucial. Raman spectroscopy is a well-established, fast, and non-destructive characterization technique for various carbon nanomaterials, including diamond-like carbons, CNTs, polycyclic aromatic hydrocarbons (PAHs) and graphene [44–46]. It is therefore expected that Raman spectroscopy could be used to fully characterize GNRs, as done with graphene. However, dimension is one of the most defining materials' parameter and we still lack a full understanding of how electrons, vibrations, and their interactions are affected by the change in the lateral dimension. Given the usually large length to width ratio, these systems can be regarded as infinite quasi-one-dimensional materials, and many similarities with graphene and CNTs are expected. On the other hand, the finite lateral size and the presence of edges introduce a molecular character, which allows making analogies with their finite counterparts, i.e., PAHs. Also, for sufficiently small length, the effect of three-dimensional confinement would make GNRs behave as elongated aromatic molecules. As such, GNRs offer a unique opportunity to study the effect of different structural parameters, such as finite width and edge-patterns, and to get insights on the evolution of the vibrational properties with the lateral dimension.

Here we report a mini-review on Raman spectroscopy of GNRs. Despite the importance of lattice vibrations for characterization purposes and transport applications, there have been relatively few works on this topic as compared to the case

of electronic properties. From an experimental point of view, most of the studies are devoted to the characterization of the high-energy region to recognize the presence of sp^2 carbon networks. Nonetheless, many works on GNRs do not report any Raman spectrum, making it difficult to compare the quality of GNRs produced by different methods. Another complication in comparing the literature results is related to the use of different experimental conditions, such as the laser wavelength, which is well known to strongly influence the Raman spectrum of sp^2 -based carbon nanostructures [44, 45, 47, 48]. From the theory side, most of the works have been instead devoted to the investigation of vibrations in ideal armchair and zigzag GNRs of nanometric width [49–57], mainly focusing on edge-related modes in different energy range. For long a direct comparison with theory was mostly inhibited due to the edge roughness and the larger widths of the samples. Only recently, after the production of atomically precise GNRs from bottom-up techniques, few combined theoretical and experimental works appeared, trying to explain the observed experimental features [34, 58, 59].

2 High-Energy Spectral Region

Figure 1 shows a selection of Raman spectra measured for ribbons produced by different methods, while Table 1 compares different Raman data reported in the literature. Note that for a meaningful comparison, we selected only measurements performed in the same excitation energy range, i.e., 514–532 nm, which are the most used laser wavelengths.

Fig. 1 Representative Raman spectra of GNRs produced with different methods: lithography (~ 30 nm width) [7]; unzipping (~ 2 nm width) [12] and bottom up (~ 1 nm width) [40]. The Raman spectrum of C_{78} is also reported for comparison [67]. All spectra have been measured with an excitation wavelength in the range 514–532 nm

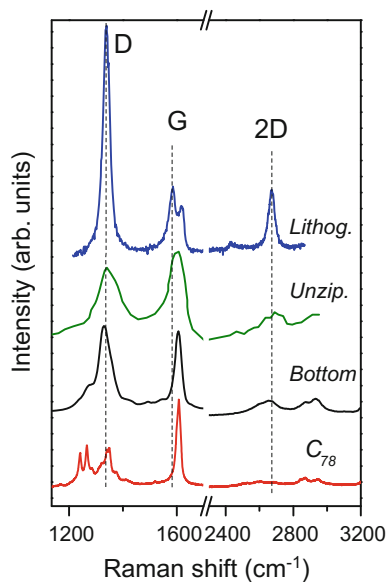


Table 1 Selection of works discussed in this review. The Raman spectrum of all GNRs is measured using an excitation wavelength in the range 514–532 nm. The third column reports the width of the ribbon (w) and every detail reported (e.g. length, thickness, quality of the edges, functional groups). The last column summarizes the main Raman spectrum features, in particular $I(D)/I(G)$ and $FWHM(D)$, which can be used to qualitatively distinguish the GNRs from defective graphene (see Fig. 2)

References	Method	Properties	Raman spectrum
[12]	Unzipping	$w < 5$ nm Edges: “Relatively smooth”	$I(D)/I(G) \sim 0.75$ $FWHM(D) \sim 100 \text{ cm}^{-1}$
[13]	Unzipping	$w = 130\text{--}250$ nm	$I(D)/I(G) \sim 1$ $FWHM(G) \sim 110 \text{ cm}^{-1}$
[14]	Unzipping	$w = 2\text{--}5$ nm Edges: “mainly zigzag”	$I(D)/I(G) \sim 0.53$ (dependent on polarization) $FWHM(D) \sim 65 \text{ cm}^{-1}$
[15]	Unzipping	$w \sim 100$ nm	$I(D)/I(G) = 0.45$ $FWHM(D) = 95 \text{ cm}^{-1}$
[16]	Unzipping	$w = 80\text{--}120$ nm	$I(D)/I(G) = 0.5\text{--}1.1$ $FWHM(D) = 70\text{--}120 \text{ cm}^{-1}$
[17]	Unzipping	$w = 20\text{--}30$ nm Oxygen-based groups	$I(D)/I(G) = 0.5$ $FWHM(D) \sim 125 \text{ cm}^{-1}$
[18]	Unzipping	$w = 50\text{--}100$ (from TEM)	$I(D)/I(G) = 0.7$ $FWHM(D) \sim 60 \text{ cm}^{-1}$
[7]	Lithography	$w = 30\text{--}500$ nm	$I(D)/I(G) \propto 1/w$ $FWHM(D)$ depends on w
[30]	CVD	$w = 10\text{--}50$ nm (by TEM) Length $> 20 \mu\text{m}$ $Sp^3 \sim 15\%$	$I(D)/I(G) \sim 0.76$ $FWHM(D) = 100 \text{ cm}^{-1}$ No 2D peak
[27]	CVD	$w = 20\text{--}300$ nm $Sp^3 = 39\%$ Thickness = 2–40 layers Edges: “relatively sharp”	$I(D)/I(G) = 1.1$ $FWHM(D) \sim 70 \text{ cm}^{-1}$ 2D peak visible
[33]	CVD	$w = 15\text{--}20$ nm Thickness = 3–5 Layers	$I(D)/I(G) \sim 1$ $FWHM(D) \sim 95 \text{ cm}^{-1}$
[28]	CVD	$w \sim 100$ nm (by SEM)	$I(D)/I(G) \sim 0.8$ $FWHM(D) \sim 120 \text{ cm}^{-1}$
[31]	Epitaxial growth on BN	$w = 15\text{--}150$ nm	$I(D)/I(G) \sim 0.6$ $FWHM(D) \sim 20 \text{ cm}^{-1}$
[36]	Bottom up	$w = 1.5\text{--}4.2$ nm (by STM) Type: 7-,14-, 24-GNR Edges: Armchair	$I(D)/I(G) \sim 1$ $FWHM(D) \sim 35 \text{ cm}^{-1}$ RBLM at 396 cm^{-1} Peak at 2000 cm^{-1} observed
[43]	Bottom up	$w \sim 1$ nm, Type: Chevron-like Edges: Armchair	$I(D)/I(G) \sim 0.55$ $FWHM(D) \sim 65 \text{ cm}^{-1}$
[34]	Bottom up	$w \ll 5$ nm Type: Chevron-like	$I(D)/I(G) \sim 0.6$ $FWHM(D) \sim 55 \text{ cm}^{-1}$
[40]	Bottom up	$w \sim 1\text{--}2$ nm Type: Cove-shaped	$I(D)/I(G) \sim 0.6\text{--}1$ $FWHM(D) \sim 50\text{--}60 \text{ cm}^{-1}$

In general the Raman spectrum of GNRs appears very similar to defective graphene, with typical defect-activated peaks [44–48], no matter the production method used. However, there could be some notable differences, depending on the GNR quality and precise structure. The first-order Raman spectrum of graphene consists of the D, G, 2D peaks, which are due to in-plane vibrations [44, 45, 60]. The G peak corresponds to the high frequency E_{2g} phonon at Γ . The D peak is due to the breathing modes of six-atom rings and requires a defect for its activation [47, 60–62]. It is activated by a resonant process [62, 63], and is strongly dispersive with excitation energy ($\sim 50 \text{ cm}^{-1}/\text{eV}$ in graphene) [48, 62, 63]. The D' peak is activated by an intra-valley and resonant process, i.e., connecting two points belonging to the same cone around K (or K'). The 2D peak is the D peak overtone, while the 2D' peak is the D' overtone.

Let us focus on the D peak. The effect of an increasing amount of defects on the Raman spectrum of graphene can be described with a phenomenological three-stage amorphization trajectory [47, 64]. In stage 1, starting from pristine graphene, the Raman spectrum evolves as follows: the D peak appears and the intensity ratio between the D and G peaks $I(D)/I(G)$ increases; the D' appears; all the peaks broaden and G and D' begin to overlap. In this stage, $I(D)/I(G)$ can be used to estimate the amount of defects [64, 65], while $I(D)/I(D')$ can be used to distinguish between different type of defects [66]. At the end of stage 1, the G and D' peaks are no more distinguishable, and $I(D)/I(G)$ starts decreasing. Stage 2 shows a marked decrease in the G peak position and strong broadening of the peaks; $I(D)/I(G)$ sharply decreases towards zero and second-order peaks are no more well defined. Stage 3 describes amorphous materials with increasing sp^3 content [47, 64, 67]. In this stage, the Raman spectrum shows an increase in the G peak position, $I(D)/I(G)$ ratio is close to zero and the G peak becomes dispersive with the excitation energy [47, 64, 67].

Many works on GNRs comment on the quality of their samples by looking at $I(D)/I(G)$ only. It is commonly believed that a decrease in $I(D)/I(G)$ should correspond to better quality GNRs (i.e., less disordered edges). However, this statement is true only for defective graphene in stage 1 and under specific conditions. First, comparison between intensity ratio is valid only if the spectra are measured under the same experimental conditions (not only excitation wavelength, but also laser polarization and type of ribbons, i.e., aligned or randomly distributed ribbons, and type of edges and thickness, i.e., single-layers or multi-layers). We remark for example that ribbons with perfect zigzag edges are expected not to show any D peak, while armchair ones are expected to always display a D peak [68, 69]. Furthermore, even by assuming that the three-stage model is valid for all GNRs, then a decrease in $I(D)/I(G)$ is not necessarily related to an increase in edge quality. Many ribbons show small $I(D)/I(G)$, but belong to stage 2, as shown by looking at both $I(D)/I(G)$ and the FWHM of the Raman peaks, e.g., of the D peak (FWHM(D)). Figure 2 collects $I(D)/I(G)$ as a function of FWHM(D) for the ribbons listed in Table 1; the blue shadow shows the amorphization trajectory, determined for defective graphene and graphene oxide (GO) [70]. Figure 2 shows that GO GNRs [26] belong to stage 2, very close to GO, as expected from their strongly

disordered nature. Furthermore, it is interesting to observe that for lithography produced ribbons with no controlled edges the cross-over between stage 1 and 2 is observed at ~ 30 nm width. Therefore, a ribbon with larger width, but belonging to stage 2 is expected to contain disorder that is not only localized at the edges. This is the case of the GNRs produced in ref 27: from the Raman spectrum $I(D)/I(G) = 1.1$ and $\text{FWHM}(D) \sim 70 \text{ cm}^{-1}$, therefore the GNRs may belong to stage 2, although they are less disordered than GO GNRs. This is in agreement with a measured sp^3 content of 39% [27]. Figure 2 also shows that methods based on CNTs unzipping can produce GNRs of very different quality, depending on the type of nanotubes and specific unzipping method used. Based on their Raman spectra, some of those GNRs belong to stage 2, and contain a relatively high amount of disorder, at least compared to GNRs of similar width produced by lithography, which are still in stage 1. Other GNRs, produced by unzipping, show very different Raman spectra, which do not belong to the amorphization trajectory. The same is observed for all GNRs produced by bottom-up approaches. This is a signature of confinement effect, which strongly changes the Raman spectrum and do not allow using the amorphization trajectory for the analysis of those nanostructures.

Let us take for comparison the Raman spectrum of an elongated aromatic molecule, such as $\text{C}_{78}\text{H}_{26}$ (C_{78}) [71]. The Raman spectrum of C_{78} shows Raman modes around 1600 and 1300 cm^{-1} , which are associated to the same eigenvectors and displacement patterns of the peaks corresponding to the G and D bands in graphene [72]. Note that unlike the case of graphene, where the D peak requires a defect for its activation, in aromatic molecules the vibrations corresponding to the D

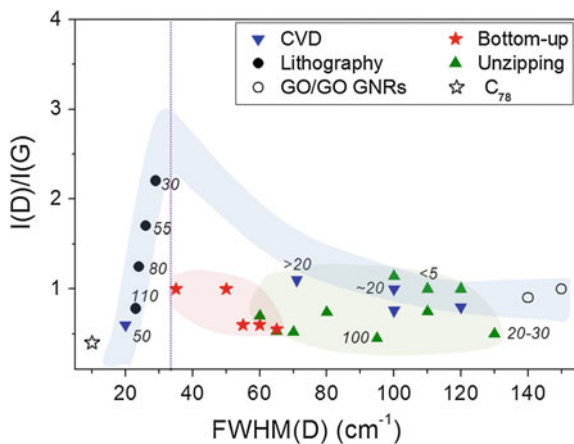


Fig. 2 $I(D)/I(G)$ vs $\text{FWHM}(D)$ for the ribbons reported in Table 1. The vertical dotted line marks the over-crossing between stage 1 and stage 2. The blue shadow represents the amorphization trajectory, starting from graphene and ending with GO. The red and green shadows collect the data for bottom-up and unzipped GNRs, respectively. The numbers close to the points refer to the width of the GNRs in nm. For in C_{78} and bottom-up ribbons we considered the most intense contribution of the D peak

peak are Raman active and do not require any defect to be seen [72]. In contrast to defective graphene, the Raman spectrum of C_{78} is characterized by several sharp (FWHM $\sim 10\text{ cm}^{-1}$) vibrational peaks in the region $1300\text{--}1400\text{ cm}^{-1}$, Fig. 1, associated to different ring vibrations [71]. The intensity of these modes is also strongly dominated by resonance effects due to the presence of a gap between the LUMO and HOMO levels [71]. This is very different from the D peak resonance-activated mode in graphene, where the resonance effects are caused by the unique electronic and phonon structure of graphene. As mentioned above, all GNRs produced by bottom-up methods do not belong to the graphene amorphization trajectory and typically show a structured D peak, with a prominent component, which reminds of the C_{78} Raman spectrum, Fig. 1. This is a signature of the peculiar character of GNRs, which are quasi-infinite in the length direction, but finite in the width direction, giving rise to fundamental and overtone modes, as theoretically predicted in Refs. [55–57]. This was demonstrated for both AGNRs [34, 59] and cove-shaped GNRs [58], from the comparison with *ab initio* density functional theory (DFT) calculations. The Raman characterization of ZGNRs, recently obtained from surface-assisted bottom-up approaches [35], is instead still absent.

Remarkably, Yamada et al. [55] investigated the phonon dispersion of A- and ZGNRs from zone folding (ZF) by using the force constants of PAH based on force-field methods, while Gillen et al. [56, 57] performed *ab initio* DFT calculations and compare their results unfolding the GNR modes onto the Brillouin zone of graphene. Both these approaches are useful to evidence differences and similarities with PAHs and graphene. In contrast to graphene, the two in-plane optical modes (transverse, TO, and longitudinal, LO) are not degenerate, even though their frequency tends to converge to that of graphene for large widths. The LO-TO splitting shows a clear dependence on the ribbon width and edge type, similar to what happens for electronic [73] and optical properties [74]. The analysis of the Raman activity also shows a dependence on the same parameters [57]. The GNR overtones reproduce quite well the phonon dispersion of graphene, especially near the Γ point. Deviations are larger near the zone edge due to the finite widths of the ribbons, and near the K point due the absence of Kohn anomalies [75] induced by the gap opening in GNRs. This analysis was extremely helpful for the interpretation of experimental observations [34, 58, 59]. In addition to G- and D-like peaks, also edge-related phonon modes also raised great interest. Among the others, a transverse edge-localized Raman active mode at $\sim 2000\text{ cm}^{-1}$, typical of non-hydrogenated AGNRs, was predicted theoretically [49, 50] and detected experimentally few years later for GNRs grown on TiC(755) [76] and more recently in bottom-up GNRs [36]. Other lower energy modes localized at the edges have been reported below 1200 cm^{-1} , and their Raman and infrared activity characterized, also in comparison with PAHs [52, 53, 55].

3 Low-Energy Spectral Region

The Raman spectrum of GNRs shows important features in the low-energy region. Specific fingerprints have been observed in this spectral region for a variety of other carbon allotropes: most notably, in the case of CNTs, a characteristic peak at low energy, associated to the radial breathing mode (RBM) of all the atoms of the structure, has been widely exploited to determine the tube diameter [45, 77]. PAHs are also characterized by breathing-like low-energy modes that can be related to their lateral size [71]. Raman signatures in this spectral region have been predicted theoretically [52, 57] for GNRs, and recently observed experimentally. Reference [34] first reported a sharp peak at 396 cm^{-1} for surface-assisted GNRs, and assigned to a Radial-Like Breathing Mode (RLBM), where all the atoms of the ribbon move in plane in directions perpendicular to the ribbon width [52]. The RLBM position is expected to depend on the GNR width, in analogy to the RBM in carbon nanotubes [45, 77]. Gillen et al. [57] calculated from first principles the frequency of the RLBM for a number of A- and ZGNRs of increasing width, mapping it onto the LA branch of graphene. The agreement, especially for sufficiently large ribbons ($w > 1.0\text{--}1.5\text{ nm}$), allows to extract an expression for the RLBM frequency based on zone folding: $\nu_{\text{RLBM}} = 3222/w$, where ν_{RLBM} is the RLBM position in cm^{-1} and the width is in Å [57]. Considering that the cut of the edge filter in standard spectrometers is around 150 cm^{-1} , ribbons with width below $\sim 2.2\text{ nm}$ should show a RLBM mode. Currently, this mode has been observed only in the Raman spectrum of bottom-up fabricated ribbons [34, 36, 40, 41, 58].

Because bottom-up approaches can generate ribbons with different geometry (e.g., cove-shaped, chevron-like, etc.), one has to be careful in extending the relation between width and RLBM position to all GNRs. One of our recent works [58] demonstrated that the relation between width and RLBM position can become rather complicated for cove-shaped GNRs, where a benzo ring periodically decorates the zigzag edge. In these GNRs the RLBM is not located exactly at the position expected using the equation above [58]. Furthermore, the RLBM does not appear as a single and sharp mode, as observed for the RBM in CNTs, but it is a broad peak, often composed by several overlapping components [58]. A number of other peaks with small intensity are also seen in the spectral range $400\text{--}700\text{ cm}^{-1}$ [58]. The RLBM peak is also slightly dispersive, although the dispersion changes with the width and edge pattern of the ribbon, in similar fashion to the D peak [58]. In general the Raman spectrum of cove-shaped GNRs is strongly sensitive to the exact edge pattern of the GNR [58]. Therefore, *ab initio* simulations have been very useful to understand how every single detail of the ribbons structure can influence the Raman features. These show that a better estimate for the RLBM frequency can be found by applying the above expression with an effective width to take into account the width modulation in cove-shaped GNRs, Fig. 3. For example for the cove-shaped 8GNR with hydrogenated edges (+H), the RLBM position is in between a 8Z-GNR and 10Z-GNR. By using the effective width, calculated as the weighted average of the different GNR widths, a good agreement between first

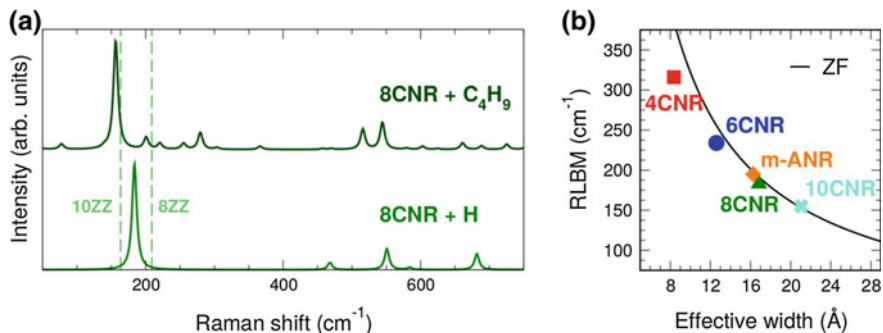


Fig. 3 **a** Simulated acoustic region of the Raman spectrum of cove-shaped carbon nanoribbons (CNRs) with $N = 8$. The spectrum is shown for both hydrogen-terminated (+H, green) and functionalized 8CNR (+C₄H₉, dark green). The dashed lines indicate the position of the RLBM for 8- and 10-ZGNRs (labeled 8-ZZ and 10-ZZ, respectively, light green) and the position of the G peak for 8-ZGNR. **b** Frequency of the RLBM calculated from first principles for several H-passivated cove-shaped GNRs is compared to the result of the zone folding (ZF) approximation (black curve) as a function of the GNR effective width. Adapted from Ref. [55]

principles simulations and the results obtained by zone folding is recovered [58], Fig. 3b. The higher frequency modes at 470–680 cm⁻¹, Fig. 3a, combining longitudinal and transverse components and not present in ZGNRs, appear in cove-shaped GNRs in view of the different periodicity along the ribbon axis introduced by the additional benzo rings at the edge. The effect of the side chains functionalizing the GNRs to improve their solubility has been also investigated by first principles calculations. Depending on the length of the alkyl chain and on the GNR width, the RLBM can be significantly modified, coupling to the modes of the chain and giving rise to several subpeaks, Fig. 3a. This can also explain the broadening of the peak observed experimentally [58].

4 Conclusions

The Raman spectrum of graphene nanoribbons is very complex due to the dual nature of GNRs, which are quasi-infinite in the length direction, but finite in the width direction. Therefore, GNRs with different width, edge pattern, and amount of defects can show very different Raman spectra. This makes Raman spectroscopy a very powerful tool for comparing different production techniques, although a systematic study, where a large variety of GNRs, produced by different methods, are studied under the same experimental conditions is currently still missing. Raman measurements on individual GNRs would be also useful to avoid any effect due to stacking; this type of sample would also allow performing resonant Raman spectroscopy, which could provide further information on electronic states and excitons in such nanostructures.

Acknowledgements The authors acknowledge A.C. Ferrari for useful discussions; I. Verzhbisky, M. Tommasini, C. Stampfer, and D. Bischoff for providing some of the Raman spectra in Fig. 1.

References

1. Novoselov, K.S., Falco, V.I., Colombo, L., Gellert, P.R., Schwab, M.G., Kim, K.: *Nature* **490**, 192–200 (2012)
2. Geim, A.K., Novoselov, K.S.: *Nature Mater.* **6**, 183–191 (2007)
3. Torres, L.E.F., Roche, S., Charlier, J.-C.: *Introduction to Graphene-Based Nanomaterials: From Electronic Structure to Quantum Transport*. Cambridge University press (2014)
4. Nakada, K., Fujita, M., Dresselhaus, G., Dresselhaus, M.S.: *Phys. Rev. B* **54**, 17954 (1996)
5. Wakabayashi, K., Fujita, M., Ajiki, H., Sigrit, M.: *Phys. Rev. B* **59**, 8271 (1999)
6. Han, M., Ozyilmaz, B., Zhang, Y., Kim, P.: *Phys. Rev. Lett.* **98**, 206805 (2007)
7. Bischoff, D., Güttinger, J., Dröscher, S., Ihn, T., Ensslin, K., Stampfer, C.: *J. Appl. Phys.* **109**, 073710 (2011)
8. Ryu, S., Maultzsch, J., Han, M.Y., Kim, P., Brus, L.E.: *ACS Nano* **5**, 4123–4130 (2011)
9. Wang, X., Dai, H.: *Nature Chem.* **2**, 661 (2010)
10. Campos, L.C., Manfrinato, V.R., Sanchez-Yamagishi, J.D., Kong, J., Jarillo-Herrero, P.: *Nano Lett.* **9**, 2600 (2009)
11. Datta, S.S., Strachan, D.R., Khamis, S.M., Johnson, A.T.C.: *Nano Lett.* **8**, 1912 (2008)
12. Wei, D., Xie, L., Lee, K.K., Hu, Z., Tan, S., Chen, W., Sow, C.H., Chen, K., Liu, Y., Wee, A. T.S.: *Nat. Commun.* **4**, 1374 (2013)
13. Kosynkin, D.V., Lu, W., Sinitskii, A., Pera, G., Sun, Z., Tour, J.M.: *ACS Nano* **5**, 968 (2011)
14. Gong, Y., et al.: *Phys Rev B* **87**, 165404 (2013)
15. Shimizu, T., Haruyama, J., Marcano, D.C., Kosinkin, D.V., Tour, J.M., Hirose, K., Suenaga, K.: *Nat. Nano* **6**, 45–50 (2011)
16. Li, Y.-S., Liao, J.-L., Wang, S.-Y., Chiang, W.-H.: *Sci. Rep.* **6**, Article number: 22755 (2016)
17. Cataldo, F., et al.: *Carbon* **48**, 2596 (2010)
18. Cano-Marquez, A.G., et al.: *Nano Lett.* **9**, 1527 (2009)
19. Jiao, L., Wang, X., Diankov, G., Wang, H., Dai, H.: *Nat. Nanotechnol.* **5**, 321 (2010)
20. Jiao, L., Zhang, L., Wang, X., Diankov, G., Dai, H.: *Nature* **458**, 877 (2009)
21. Elías, A.L., Botello-Méndez, A.R., Meneses-Rodríguez, D., Jehová González, V., Ramírez-González, D., Ci, L., Muñoz-Sandoval, E., Ajayan, P.M., Terrones, H., Terrones, M., *Nano Lett.* **10**, 366 (2010)
22. Zhu, Y., Tour, J.M.: *Nano Lett.* **10**, 4356 (2010)
23. Magda, G.Z., Jin, X., Hagymási, I., Vancsó, P., Osváth, Z., Nemes-Incze, P., Hwang, C., Biró, L.P., Tapasztó, L.: *Nature* **514**, 608 (2015)
24. Li, X., Wang, X., Zhang, L., Lee, S., Dai, H.: *Science* **319**, 1229 (2008)
25. Ren, X.D., Liu, R., Zheng, L.M., Ren, Y.P., Hu, Z.Z., He, H.: *Appl. Phys. Lett.* **108**, 071904 (2016)
26. Higginbotham, A.L., Kosynkin, D.V., Sinitskii, A., Sun, Z., Tour, J.M.: *ACS Nano* **4**, 2059 (2010)
27. Campos-Delgado, J., et al.: *Nano Lett.* **8**, 2773 (2008)
28. Zhang, J., et al.: *J. Alloys and Comp.* **649**, 933 (2015)
29. Suzuki, H., et al.: *Nature. Commun.* **7**, 11797 (2016)
30. Sokolov, A.N., et al.: *Nature. Commun.* **4**, 2402 (2013)
31. Lu, X., et al.: *Appl. Phys. Lett.* **108**, 113103 (2016)
32. Jacobberger, R.M., et al.: *Nature Comms* **6**, 68006 (2015)
33. Martin-Fernandez, I., Wang, D., Zhang, Y.: *Nano Lett.* **12**, 6175 (2012)
34. Cai, J., Ruffieux, P., Jaafar, R., Bieri, M., Braun, T., Blankenburg, S., Muoth, M., Seitsonen, A.P., Saleh, M., Feng, X., et al.: *Nature* **466**, 470–473 (2010)

35. Ruffieux, P., Wang, S., Yang, B., Sánchez-Sánchez, C., Liu, J., Dienel, T., Talirz, L., Shinde, P., Pignedoli, C.A., Passerone, D., Dumszlaff, T., Feng, X., Müllen, K., Fasel, R.: *Nature* **531**, 489–492 (2016)
36. Huang, H., et al.: *Scientific Reports* **2**, 983 (2012)
37. Fogel, Y., Zhi, L., Rouhanipour, A., Andrienko, D., Rader, H.J., Mullen, K.: *Macromolecules* **42**, 6878 (2009)
38. Dossel, L., Gherghel, L., Feng, X., Mullen, K.: *Angew. Chem. Int. Ed.* **50**, 2540 (2011)
39. Schwab, M.G., Narita, A., Hernandez, Y., Balandina, T., Mali, K.S., De Feyter, S., Feng, X., Muellen, K.: *J. Am. Chem. Soc.* **134**, 18169 (2012)
40. Narita, A., Feng, X., Hernandez, Y., Jensen, S.A., Bonn, M., Yang, H., Verzhbitskiy, I.A., Casiraghi, C., Hansen, M.R., Koch, A.H.R., Fytas, G., Ivasenko, O., Li, B., Mali, K.S., Balandina, T., Mahesh, S., De Feyter, S., Muellen, K.: *Nat. Chem.* **6**, 126 (2014)
41. Narita, A., Verzhbitskiy, I.A., Frederickx, W., Mali, K.S., Jensen, S.A., Hansen, M.R., Bonn, M., De Feyter, S., Casiraghi, C., Feng, X., Müllen, K.: *ACS Nano* **8**, 11622 (2014)
42. Gao, J., Uribe-Romo, F.J., Saathoff, J.D., Arslan, H., Crick, C.R., Hein, S.J., Itin, B., Clancy, P., Dichtel, W.R., Loo, Y.-L.: *ACS Nano* **10**, 4847 (2016)
43. Vo, T., Shekhirev, M., Kunkel, D.A., Morton, M.D., Berglund, E., Kong, L., Wilson, P.M., Dowben, P.A., Enders, A., Sinitskii, A.: *Nat. commun.* **5**, 3189 (2014)
44. Ferrari, A.C., Robertson, J.: Raman spectroscopy of amorphous, nanostructured, diamond-like carbon, and nanodiamond. *Phil. Trans. R. Soc. Lond. A* **362**, 2477 (2004)
45. Jorio, A., Saito, R., Dresselhaus, G., Dresselhaus, M.S.: *Raman Spectroscopy in Graphene Related Systems*. Wiley-VCH Verlag GmbH (2011)
46. Casiraghi, C.: Raman spectroscopy of graphene. In: *Spectroscopic Properties of Inorganic and Organometallic Compounds: Techniques, Materials and Applications*, vol. 43, pp. 29–56. The Royal Society of Chemistry (2012)
47. Ferrari, A.C., Robertson, J.: *Phys. Rev. B* **64**, 075414 (2001)
48. Eckmann, A., Felten, A., Verzhbitskiy, I., Davey, R., Casiraghi, C.: *Phys. Rev. B* **88**, 35426 (2013)
49. Igami, M., Fujita, M., Mizuno, S.: *Appl. Surf. Sci.* **130–132**, 870 (1998)
50. Kawai, T., Miyamoto, Y., Sugino, O., Koga, Y.: *Phys. Rev. B* **62**, R16349 (2000)
51. Yamamoto, T., Watanabe, K., Mii, K.: *Phys. Rev. B* **70**, 245402 (2004)
52. Zhou, J., Dong, J.: *Appl. Phys. Lett.* **91**, 173108 (2007)
53. Vandescuren, M., Hermet, P., Meunier, V., Henrard, L., Lambin, Ph.: *Phys. Rev. B* **78**, 195401 (2008)
54. Malola, S., Hakkinen, H., Koskinen, P.: *Eur. Phys. J. D* **52**, 71 (2009)
55. Yamada, M., Yamakita, Y., Ohno, K.: *Phys. Rev. B* **77**, 054302 (2008)
56. Gillen, R., Mohr, M., Maultzsch, J., Thomsen, C.: *Phys. Rev. B* **80**, 155418 (2009)
57. Gillen, R., Mohr, M., Maultzsch, J.: *Phys. Rev. B* **81**, 205426 (2010)
58. Verzhbitskiy, I., et al.: *Nano Lett.* **16**, 3442 (2016)
59. Yang, W., Lucotti, A., Tommasini, M., Chalifoux, W.A.: *J. Am. Chem. Soc.* **138**, 9137–9144 (2016)
60. Tuinstra, F., Koenig, J.L.: *J. Chem. Phys.* **53**, 1126–1130 (1970)
61. Ferrari, A.C., Robertson, J.: *Phys. Rev. B* **61**, 14095–14107 (2000)
62. Thomsen, C., Reich, S.: *Phys. Rev. Lett.* **85**, 5214–5217 (2000)
63. Baranov, A.V., et al.: *Opt. Spectroscopy* **62**, 612–616 (1987)
64. Cançado, L.G., et al.: *Nano Lett.* **11**, 3190–3196 (2011)
65. Martins Ferreira, E.H., Moutinho, M.V.O., Stavale, F., Lucchese, M.M., Capaz, R.B., Achete, C.A., Jorio, A.: *Phys. Rev. B* **82**, 125429 (2010)
66. Eckmann, A., Felten, A., Mishchenko, A., Britnell, L., Krupke, R., Novoselov, K.S., Casiraghi, C.: *Nano Lett.* **12**, 3925 (2012)
67. Casiraghi, C., Ferrari, A.C., Robertson, J.: *Phys. Rev. B* **72**, 085401 (2005)
68. Casiraghi, C., Hartschuh, A., Qian, H., Piscanec, S., Georgi, C., Fasoli, A., Novoselov, K.S., Basko, D.M., Ferrari, A.C.: *Nano Lett.* **9**, 1433 (2009)
69. Cançado, L.G., et al.: *Phys. Rev. Lett.* **93**, 247401 (2004)

- 70. Stankovich, S., et al.: Carbon **45**, 1558 (2007)
- 71. Maghsoumi, A., et al.: J. Raman Spectrosc. **46**, 757 (2015)
- 72. Castiglioni, C., Tommasini, M., Zerbi, G.: Raman spectroscopy of polyconjugated molecules and materials: confinement effect in one and two dimensions. Phil. Trans. R. Soc. Lond. A **362**, 2425–2459 (2004)
- 73. Son, Y.-W., Cohen, M.L., Louie, S.G.: Phys. Rev. Lett. **97**, 216803 (2006)
- 74. Prezzi, D., Varsano, D., Ruini, A., Marini, A., Molinari, E.: Phys. Rev. B **77**, 041404(R) (2008)
- 75. Piscanec, S., Lazzeri, M., Mauri, F., Ferrari, A.C., Robertson, J.: Phys. Rev. Lett. **93**, 185503 (2004)
- 76. Tanaka, T., Tajima, A., Moriizumi, R., Hosoda, M., Ohno, R., Rokuta, E., Oshima, C., Otani, S.: Solid State Commun. **123**, 33 (2002)
- 77. Rao, A.M., Richter, E., Bandow, S., Chase, B., Eklund, P.C., Williams, K.A., Fang, S., Subbaswamy, K.R., Menon, M., Thess, A., Smalley, R.E., Dresselhaus, G., Dresselhaus, M. S.: Science **275**, 187 (1997)

GraphITA

Selected papers from the Workshop on Synthesis,
Characterization and Technological Exploitation of
Graphene and 2D Materials Beyond Graphene

Morandi, V.; Ottaviano, L. (Eds.)

2017, VIII, 221 p. 86 illus., 82 illus. in color., Hardcover

ISBN: 978-3-319-58132-3